Optimization of an electron beam lithography instrument for fast, large area writing at 10 kV acceleration voltage

Martin M. Greve, and Bodil Holst

Citation: Journal of Vacuum Science & Technology B, Nanotechnology and Microelectronics: Materials, Processing, Measurement, and Phenomena **31**, 043202 (2013); doi: 10.1116/1.4813325

View online: https://doi.org/10.1116/1.4813325

View Table of Contents: http://avs.scitation.org/toc/jvb/31/4

Published by the American Vacuum Society

Optimization of an electron beam lithography instrument for fast, large area writing at 10 kV acceleration voltage

Martin M. Greve[a)]
Department of Physics and Technology, University of Bergen, Allègaten 55, 5007 Bergen, Norway and EnSol AS, Apeltunveien 2, Nesttun, 5222 Bergen, Norway

Bodil Holst[b)]
Department of Physics and Technology, University of Bergen, Allègaten 55, 5007 Bergen, Norway

(Received 28 February 2013; accepted 17 June 2013; published 23 July 2013)

Electron beam lithography (EBL) is a maskless lithography technique used in numerous applications for fabrication of ultrahigh-resolution photolithography masks. The main disadvantage of EBL is that it is time-consuming, requiring the pattern to be written in a successive fashion. Various approaches are used to lower the write time. Throughput-oriented EBL instruments used in industrial applications typically apply a very high acceleration voltage (≥50 kV). However, in many research environments, more cost-effective instruments are used. These tools are usually optimized for high-resolution writing and are not very fast. Hence, they are normally not considered very suitable for writing large-scale structures with high pattern densities, even for limited resolution applications. In this paper, the authors show that a carefully considered optimization of the writing parameters in an EBL instrument (*Raith e_LiNE*) can improve the writing time to more than 40 times faster than commonly used instrument settings. The authors have applied the optimization procedure in the fabrication of high-precision photolithography masks. Chrome photolithography masks, 15 mm in diameter with a write resolution of 200 nm, were routinely produced during overnight exposures (less than 9 h). The write time estimated by the instrument software for most commonly used settings was close to 14 days. A comparison with conventional chrome masks fabricated using a high-resolution (128 000 dpi) photolithography mask printer showed that our pattern definition is significantly better. [http://dx.doi.org/10.1116/1.4813325]

I. INTRODUCTION

Several maskless lithography methods exist: electron beam lithography (EBL), direct laser writing[1,2] and interference lithography[3] are among the ones most widely used. Other techniques such as focus ion beam lithography[4] and dip pen lithography[5] are becoming increasingly important. For an overview of different maskless lithography techniques, see Refs. 6 and 7.

EBL is widely used in many research areas dealing with nanotechnology, with the ability to write patterns with very high resolution down to a few nanometers.[8] In the EBL writing process, a tightly focused beam of electrons exposes a resist, which is then developed. The resist pattern can then be further processed in various ways to create the final structure.[9] Since the wavelength of the electrons is in the range of picometers or less, EBL is not diffraction-limited under typical operating conditions.[10] The main limitations on achieving high resolution in an EBL system are the resists and the consecutive processing steps.[11] One of the most widely used resists is the positive resist poly(methyl methacrylate) (PMMA), mainly due to the very high resolution (can be down to less than 10 nm linewidths).[12]

In EBL, the patterning time is mainly spent in three ways: Resist exposure, stage movement (for structures exceeding the size of a single write-field), and electron beam settling. The settling time is a delay typically embedded in the EBL software to ensure that the beam is stable at each new location. Space charge effects lead a physical limit to the maximum achievable beam current. This sets an upper limit for the patterning time in serial exposure with a single beam. Shaped beams and multibeam exposure tools can be faster because the overall beam current can be higher.[13,14]

To increase the write speed of any EBL system, the exposure time and the idle time of the system should both be minimized. It has been reported that for newer resists, such as the negative tone resist SU-8, the sensitivity is as high as 3.6 μC/cm^2 when exposed by a 50 kV electron beam.[15] This is almost 100 times more sensitive than PMMA. It should be noted, however, that the ultimate resolution achieved for SU-8 is not as high as for PMMA.[16,17]

Medium-resolution EBL, in the range of 200 nm, has not been a main research focus compared to ultrahigh-resolution EBL, which exploits the ultimate patterning performance of EBL. However, there are some cases where fast writing and large-area structures are more important than ultrahigh resolutions, for example, certain types of photolithography masks or microfluidic patterns. In this article, we systematically test how the writing speed can be optimized in order to increase the capability of EBL for writing over large areas. The experiments were performed with a Raith e_LiNE EBL tool, a common instrument in research institutions.

[a)]Electronic mail: martin.greve@ift.uib.no
[b)]Electronic mail: bodil.holst@ift.uib.no

The aim of the present work is to increase the writing speed of our EBL system as much as possible in order to manufacture large optical elements (photolithography masks) exploiting a so-called "binary radially sinusoidal zone plate" pattern recently developed by our group.[18] The aim was to determine parameters, allowing cm^2-area writing, within an acceptable time frame (less than 12 h) and with a precision better than what is commercially available with standard printing production techniques (typically 1.5 μm).

II. WRITE-TIME OPTIMIZATION CRITERIA

The time it takes to write an area in an EBL instrument can be approximated by the following equation:

$$\text{Dose}[\mu\text{C}/\text{cm}^2] \times \text{Area}[\text{cm}^2] = \text{Time}[\text{s}] \times \text{Beamcurrent}[\text{nA}], \quad (1)$$

where Dose is the clearance dose of the resist, Area is the area to be exposed, Time is the total time needed for exposing the area, and Beamcurrent is the current of the electron beam. It should be noted that the Area here corresponds only to the area illuminated by the beam, and not the area of the total write-field. The clearance dose is a measure for the number of electrons needed for fully exposing 1 cm^2 so that it can be removed in the subsequent development step. Here we assume a simple, binary exposure setup, where the resist is either removed or kept. Gray-scale exposure is also possible, but this is not discussed in this paper. Note that stage movement and beam settling times are not taken into account in Eq. (1). When our Raith e_LiNE is set to typical settings (see Table I), using a 10 kV acceleration voltage and a 30 μm aperture, the beam current is about 0.12 nA (this will vary depending on the gun settings and the state of the filament/electron source). With this beam current, it will take approximately 10 days to expose an area of 1 cm^2 in PMMA, with a clearance dose of around 100 $\mu C/cm^2$, not taking into account stage movement and beam settling time. Occupying an EBL tool for such a long period of time is clearly not acceptable in any nanostructuring laboratory due to the time pressure on such facilities. Furthermore, additional overhead time has to be considered for readjustment of the dwell time and the stage position. In the following, we describe how the various parameters can be optimized to minimize the writing time.

TABLE I. Left column shows typical settings provided for writing with the Raith e_LiNE instrument. In the right column are the settings we used for fast, large-area writing. Note the beam current can vary considerably depending on the gun settings and the state of the filament.

	Standard settings	Fast write settings
Aperture size	30 μm	120 μm
Acceleration voltage	10 kV	10 kV
Measured beam current	0.12 nA	6.2 nA
High current mode	Off	On
Scan mode	Linescan	Meanderscan
Writefield size	100 μm	1000 μm

A. Determining the acceleration voltage

The clearance dose of a resist increases with the acceleration voltage.[19] This is because, at lower acceleration voltages ($\leq$10 kV), the forward-scattered electrons will a more efficient energy transfer to the resist, leading to a lower clearance dose requirement, but at the cost of a broadening of the incident beam spot and higher line roughness.[20,21]

The necessary clearance dose is also highly dependent on the developer type and development process.[17,22] We determined the clearance dose by writing a dose matrix for different acceleration voltages and using a standard development process described in Sec. IV. Following this procedure, we selected clearance doses of 110 and 450 $\mu C/cm^2$ for the two acceleration voltages 10 and 30 kV (highest acceleration voltage for the Raith e_LiNE system), respectively. The corresponding beam currents for commonly used settings were 0.12 and 0.21 nA (see Table I), respectively, and between the two commonly used acceleration voltages tested in our laboratory, 10 kV offered the faster exposure.

B. Choosing the collimating aperture size

The electron beam can be collimated and current-limited by interchangeable apertures in the beam line. From Eq. (1), it can be seen that for a set pattern and a given resist with specific sensitivity, the only parameter that directly can decrease the total write time is the beam current. We increased the beam current by switching from the standard 30 μm diameter to the largest available 120 μm diameter collimating aperture, allowing more electrons emitted from the filament to reach the sample. A collimating aperture in the electron column is a standard feature of an electron microscope. The purpose of the aperture is to change the numerical aperture for the incident beam. A smaller aperture means a smaller numerical aperture and, hence, a larger field of depth. It was not possible to obtain precise information concerning the numerical aperture from Raith, but they stated that the field of depth typically changed from approximately 10 to 1–2 μm when switching between the 30 and 120 μm diameter apertures, respectively.[23] So, for the resolution in the 200 nm range applied here, it is a safe assumption that the size of the collimating aperture irrelevant. The beam current is increased to about 3.1 nA for an acceleration voltage of 10 kV, close to 30 times higher than for the standard aperture. From Eq. (1), the writing time is inversely proportional to the beam current, so the write time is expected to decrease about 30 times.

C. Enabling high current mode

Raith offers what is called a "high current" mode, where the focusing properties of the condenser lens are changed, resulting in an overall smaller, parallel beam[24] (see Fig. 1). This mode will approximately double the beam current. The ultimate resolution will decrease slightly due to space charge effects,[25] but the smaller, parallel beam will increase the depth of focus significantly.[24] We measured a beam current of 6.2 nA for the high current mode when the acceleration

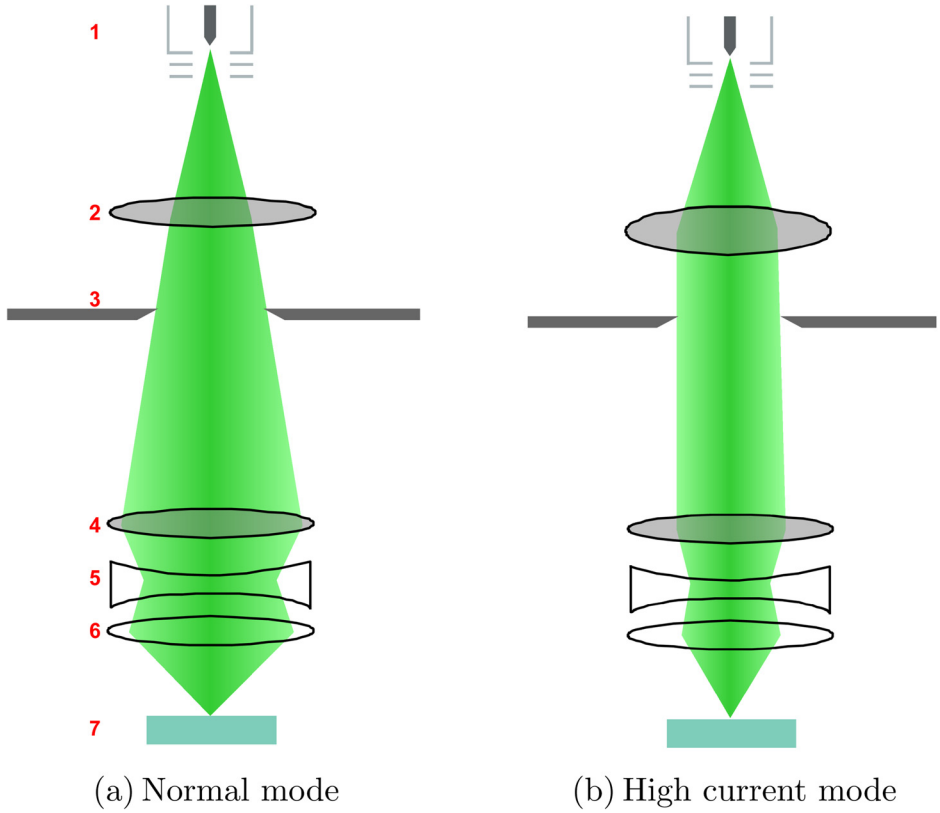

FIG. 1. (Color online) Beam paths of the two different current modes. The numbers indicate the position of the different parts in the SEM column. 1. Filament, 2. Condenser lens, 3. Collimating aperture, 4–6. Additional lenses, and 7. Specimen. The focal length of the condenser lens is changed in the high current mode (b). This leads to a narrower beam with higher current density. Note that the angular spread of the focused beam on the sample is smaller in the high current mode, thus increasing the depth of field. Figures are reproduced with permission from Raith.

voltage was 10 kV and the 120 μm diameter collimating aperture was used.

D. Write-field size

A typical write-field size is 100 μm × 100 μm. We selected a large write-field of 1000 μm × 1000 μm (where the largest available is 2000 μm × 2000 μm), resulting in the pattern being reproduced from a 100 times fewer write-fields. Hence, the sample stage moving time and the following settling time for the stage will be decreased by a factor of 100.

There are several disadvantages in using a larger write-fields. The minimum step size will decrease due to the limited addressable resolution defined by the digital-to-analog-converter (DAC) of the pattern generator (in our case 16 bit). The limit in the addressable step size of the EBL, for a 1000 μm × 1000 μm write-fields, will, however, still very small [see Eq. (2)]. For the 16-bit DAC used in the Raith e_LiNE and the large write-fields, we can calculate the minimum addressable step size as

$$\text{Step size} = \frac{1000\,\mu\text{m}}{2^{16}} \approx 16\,\text{nm}, \tag{2}$$

where the denominator is the available number of DAC bits. Increasing the step size to the value of the beam spot

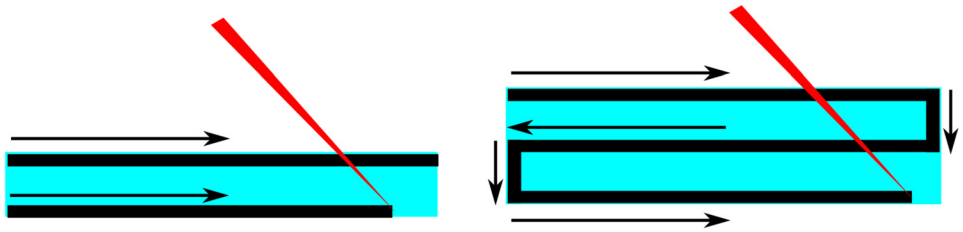

FIG. 2. (Color online) Figure illustrating the two different ways of moving the beam. In the line mode, the beam is blanked when moved between each line, and a dynamic compensation is enabled at the start and end of each line. The meander mode writes the full structure from top to bottom in one go, only blanking when passing areas not to be exposed and when stitching write-fields.

diameter or beyond will lead to line-edge roughness and a broken pattern. Other disadvantages of larger write-fields are defocusing at the write-fields edges leading to pattern placement errors, stitching errors, and loss of critical dimension control.

E. Write mode

There are generally two modes of moving the beam inside one write-fields: raster and vector scan. Raster scan is the simpler approach, but usually more time-consuming. In a raster scan, the beam is scanned over the full write-field and unblanked when passing over areas to be exposed. The more technically challenging vector scan moves the beam directly to each area to be exposed and only scans over the areas. We note that the time saved by using a vector scan will depend strongly on the type of pattern to be made. A very regular pattern, with many small, open and closed areas, may even be written more quickly using the raster scan approach, since a larger beam settling time is typically needed for vector scanning.

The write mode of the beam determines how the electron beam moves during the patterning process. Various write modes exist for different instruments and this should be considered for each writing application. The optimum write mode will depend on the pattern shape, the ratio of exposed to unexposed area, whether gray-scale exposure is desired, etc. The standard write mode is called line mode. Here, the whole pattern is written as a series of lines, all commencing from the same side [see Fig. 2(a)]. The beam will be blanked by the beam-blanker when moving between lines, and at the start of each new line a short settling time is allowed for the beam. For the e_LiNE, the settling time can be set manually. The default setting depends on the jump distance of the beam 50 ms/mm for our instrument. In addition, what is called "dynamic compensation" is normally turned on in the line mode. This will increase the precision of the pattern edge. When a large number of lines are to be written, this seemingly small settling time and the dynamic compensation add up to a significant amount of system idle time.

This can be avoided by using the "meander" write mode when patterning. This mode will not blank the beam when the end of a line is reached. Instead, it will move the beam directly to the subsequent line, and continue writing the next line in the opposite direction [see Fig. 2(b)]. Both the time spent blanking the beam when moving between lines and the settling times are avoided. This leads to a ≈150% improvement in write time. Meander mode is not the standard setting for writing, as it cannot be used with the dynamic compensation and it will expose when moving between lines, as illustrated in Fig. 2(b). It should be noted that the meander mode can sometimes lead to a shift between pattern parts written from the different sides; however, we did not observe this phenomenon.

F. Beam speed and step size

Patterns are designed and handled in the e_LiNE design software using a GDSII module optimized for Raith lithography system. The GDSII format is commonly used in the integrated circuit industry. Other pattern file formats, such as bitmaps, can be imported. The simplest mode of importing a bitmap into the e_LiNE software is "bitmap as reference." When using the line or meander mode, in combination with the 'bitmap as reference' format, the beam will scan the full write-field, unblanking and blanking for exposing or not exposing, respectively, using the pattern bitmap as reference. The writing resolution will be determined by a grid superimposed on the imported reference pattern. The grid is defined by setting the step size in x- and y-directions (see Fig. 3). Typically, the same step size is used in both directions. For simplicity, a square in this superimposed grid is referred to as "grid pixel," and an element in the reference pattern bitmap is referred to as a "pattern pixel" in the rest of this paper.

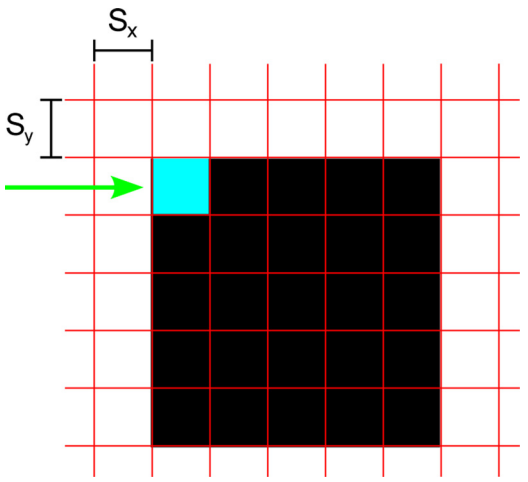

FIG. 3. (Color online) Black square is a pattern pixel: a single pixel in the reference pattern bitmap. The grid is the overlying step size defined grid pixels, where S_x and S_y represent the user-defined step sizes in x- and y-directions. The pixel area pointed to by the arrow indicates the first patterned grid pixel and thus represents the writing resolution. The beam will move in the direction indicated by the arrow. When passing over a grid pixel, the beam is moved in a sweeping pattern defined by Raith so that all of the grid pixel area is exposed evenly with the correct dose. The beam pattern movement over the grid pixel will add up to the dose and the dwell time defined in the software. When the beam is passing over the white area of the grid, the beam will be blanked by the beam blanker.

The step size in combination with the clearance dose and beam current now allow us to determine a theoretical upper limit for write speed. The real limit is likely to be considerably lower. The speed with which a single grid pixel can be addressed is determined by the speed of the pattern

TABLE II. Patterning settings used for patterning the chrome mask structure (Ref. 18). The beam speed and dwell time will vary depending on the measured beam current and the step size and dose set by the user.

Parameter	Value
Beam step size	0.2 μm
Beam speed	28.2 mm/s
Dose	110 μC/cm^2
Dwell time	0.007096 ms

TABLE III. Time to expose a single grid pixel and the time to expose a full area (15 × 15 mm) is estimated for a beam current of 6.2 nA for a theoretical Fast Beam (FB) speed using the settings calculated in Eqs. (4) and (5), and for the Actual Parameters (AP) we used in our experiment shown in Table II. The single grid pixel is the time for exposing one grid pixel and the full area is the time to expose a single pixel times the number of pixels extended over the full area. The actual writing time for our structure using AP settings was about 8 h and 45 min. Note that the reason the actual writing time is much shorter than the time listed for AP in the table is that less than half the full area is exposed when our structure is written.

Parameter mode	Single grid pixel	Full area
Fast beam (15.8 nm step size)	$50 \cdot 10^{-9}$ [s/pixel]	$50 \cdot 10^{-9}$[s/pixel] $\cdot (8.93 \cdot 10^5)^2$[pixel] $\approx$ 39 900 [s] $\approx$ 11.1[h]
Actual parameters (200 nm step size)	$7.1 \cdot 10^{-6}$ [s/pixel]	$7.1 \cdot 10^{-6}$[s/pixel] $\cdot (7.5 \cdot 10^4)^2$[pixel] $\approx$ 39 900 [s] $\approx$ 11.1[h]

generator. The pattern generator thus defines a minimum "dwell time" for a pixel. Our Raith e_LiNE has a 20 MHz pattern generator, leading to a minimum dwell time of 50 ns. By rewriting Eq. (1) for one grid pixel (assuming same step size in x and y directions) and the dwell time, Eq. (3) is obtained:

$$\text{Dose} = \frac{\text{Beamcurrent} \cdot \text{Dwelltime}}{\text{Stepsize}^2}, \tag{3}$$

where the Dwelltime is the time needed, at a given beam current, for the beam to mediate the clearance dose to the resist. We can find the smallest step size theoretically possible for the minimum dwell time and the experimental values in Table II.

$$\text{Stepsize} = \sqrt{\frac{\text{Beamcurrent} \cdot \text{Dwelltime}}{\text{Dose}}} = \sqrt{\frac{6.2\,\text{nA} \cdot 50\,\text{ns}}{110\,\mu\text{C/cm}^2}} = 16.8\,\text{nm}. \tag{4}$$

The relationship between the beam speed and the step size is shown in Eq. (5). We now find the highest theoretical beam speed for the system to be

$$\text{Beamspeed} = \frac{\text{Stepsize}}{\text{Dwelltime}} = \frac{17\,\text{nm}}{50\,\text{ns}} = 340\,\text{mm/s}. \tag{5}$$

Raith recommends a maximum beam speed of 10 mm/s. Excessively high beam speeds can lead to pattern artifacts and imprecisions. However, communications with Raith revealed that beamspeed is write-mode dependant and that in reality it is often possible to go to considerably higher speeds when using the line or meander modes.

An important point is that the time it takes to write a specific area will, in theory, not be affected by the beam speed or the step size, but only by the fraction of the area that needs to be exposed. In practice, both beam speed and step size are likely to have an effect. The theoretical write times for two different beam speeds and step sizes to fully expose a 15 mm^2 area are shown in Table III.

The pattern pixel size in our bitmap pattern was 900 nm. We chose a step size of 200 nm in a compromise to ensure good pattern definition, while oversampling the pattern pixels and avoiding excessive beam speeds. It should be noted that since we imported the "bitmap as reference," the resolution was limited by the basic step size of the system (which is 16 nm for a 1000 -μm write-field compared to the 200-nm step size set in the software). If the bitmap had been "imported as elements," the selected step size would be the limiting resolution, which could lead to patterning errors if it did not match the pattern design specifications well. The selected step size led to a beam speed of about 28 mm/s (see Table II), and no patterning artifact issues were observed. It should be possible to go to lower step sizes in many cases. In Fig. 4, an image of the entire chrome mask is shown, and an optical microscope image comparing details of the EBL-fabricated mask with the actual pattern template is shown in Fig. 5. We did a series of line width tests (not shown), using these settings, to confirm that we achieved the 200 nm line width limited by the step size.

III. CHALLENGES USING THE FAST-WRITE APPROACH

Writing large patterns means that several write-fields are used, which must be stitched together. The precision of the beam placement upon moving from one write-field to another

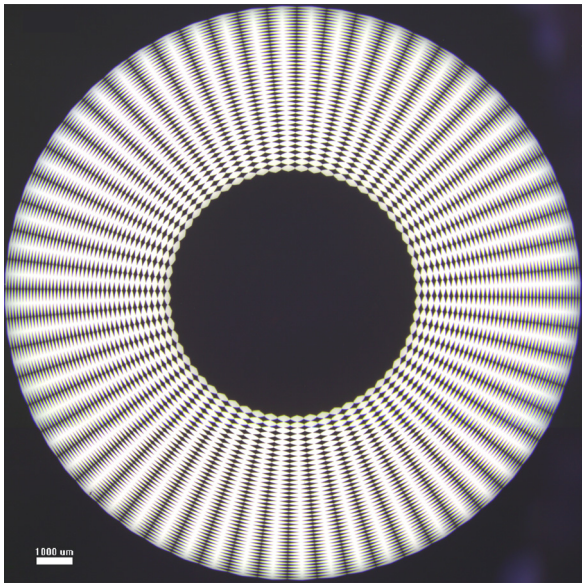

FIG. 4. (Color online) Stereo microscope image of our EBL-written chrome mask structure. The diameter of the pattern is 15.8 mm. A higher-magnification optical microscopy image of chrome mask structure details can be seen in Fig. 5(a).

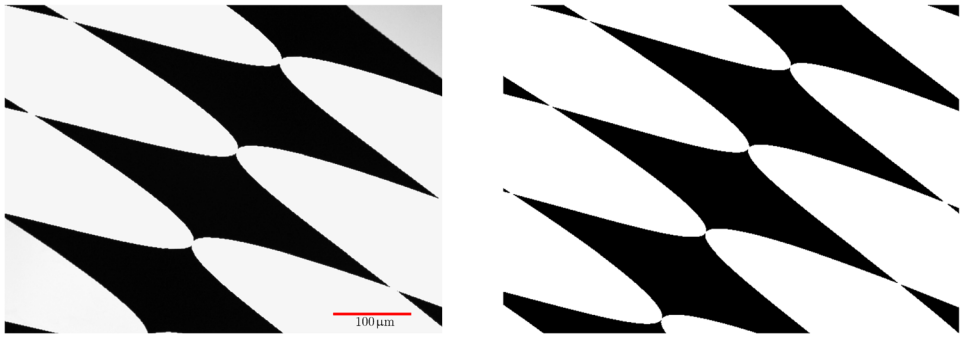

(a) Optical microscopy image of the EBL produced chrome mask structure

(b) Section of the bitmap pattern used for writing the chrome mask structure

FIG. 5. (Color online) Comparison of the EBL-fabricated chrome mask (a) and a cut-out of the computer-generated bitmap used for writing the chrome mask (b). The images are approximately to-scale, and the resolution of the bitmap is 900 nm. It can be seen that the pixelation of the bitmap is reproduced in the EBL mask.

is ultimately determined by the precision of the stage movement. For the Raith e_LiNE, the stage is positioned using laser interferometers, ensuring a position accuracy of 1 nm. The beam placement accuracy is calibrated for each write using beam-tracking and write-field alignment procedures. Using high beam currents limits the image quality severely due to charging effects mainly in the PMMA. This constitutes a significant challenge in the alignment procedure, and could potentially lead to pronounced stitching errors.

We learned that for the highest currents, in the range of 6 nA accelerated at 10 kV and using the secondary electron detector, SE2 [Everhart-Thornley (E-T) type], the PMMA became "transparent" to the electrons meaning that the underlying chrome layer could be seen through the PMMA (see Fig. 6). Significantly better beam focus and image quality were achieved, leading to much higher accuracy in write-fields stitching. We investigated the origin of this useful effect in more detail by taking a series of images with the detector set to negative voltages (−100 to −250 V), thereby repelling all secondary electrons. Even with this negative bias, the chrome layer could still be seen. This indicates that the underlying chrome is visible due to back-scattered electrons (BSE), tying in with the fact that a high beam current should give an increased BSE signal reaching the SE2 detector. The PMMA charging is not necessarily reduced, but is not sufficiently high to distort the high-energy back scattered electrons. For this reason, the SE2 detector was selected over the InLens, both for imaging and aligning.

IV. CHROME PHOTOLITHOGRAPHY MASK FABRICATION PROCEDURE

We used thin borosilicate glass slides as substrates (approx. 190 μm thick). The glass slides were solvent-cleaned by sonicating them in two different baths for 6 min each, first in 2-propanone (acetone), followed by isopropyl alcohol (IPA). After each bath, the slides were rinsed with IPA and then blown dry using pressurized nitrogen (N_2). Next, the slides were rinsed by streaming deionized water over them for 2 min, blown dry using N_2, and baked for 5 min at 115 °C. Then each glass slide was coated with an approximately 100 nm thick layer of chromium using an electron beam evaporator (Temescal FC-2000). The thickness was chosen to achieve an optical density greater than 2.5.[26] A 160 nm thick layer of PMMA was spin-coated on top of the chromium, and the substrate was soft-baked for 5 minutes at 175 °C. Then followed the EBL exposure as described in the previous section. After the EBL exposure, the exposed PMMA was removed by submerging the sample in the developer, [1:3] methyl isobutyl ketone (MIBK):(IPA), for 2 minutes. Immediately after development, the sample was flushed with IPA.

A chrome etchant (Transene Company Inc. Chrome Etch 1020) was heated to 40 °C to give an etch rate of 40 Å/s. The sample was submerged in the etchant, and the chrome not masked by PMMA was removed fully after being etched for approximately 30 seconds. Finally, the PMMA mask was stripped using acetone.

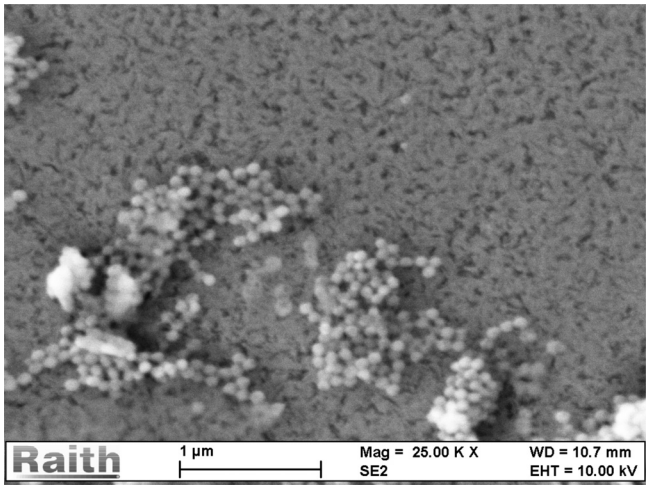

FIG. 6. Image showing the underlying chrome film (visible as a textured layer) taken using the fast write settings in Table I. The polystyrene beads are sitting on top of the PMMA, and the PMMA itself is transparent. This significantly improves the focus quality of the beam and the write-field alignment.

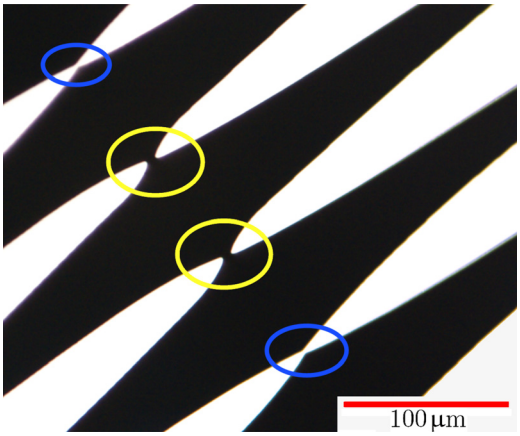

FIG. 7. (Color online) Optical microscopy image of a commercially produced chrome mask. The pattern is made using the same image file as for the ones fabricated using EBL [see Fig. 5(a)]. The circles are drawn to show tapering lines, which have opened more than they should. The two circles in the middle show tapering lines, which have generated closed areas.

V. COMPARISON WITH COMMERCIALLY AVAILABLE PHOTOMASKS

To further evaluate the EBL fast writing performance, we purchased the highest resolution commercial photolithography mask available, which is produced using a high-resolution (128 000 dpi) photolithography mask printer. The test pattern sent off for printing had the same resolution as the EBL bitmap pattern file. In the midst of working with the supplier, several constraints were encountered. The first limitation was the minimum linewidth for the photomask printer, which was approximately 1.8 μm. The minimum linewidth increased for curved lines. Also, tapering lines were expected to end prematurely or fully close for distances less than about 1.5 μm (examples of this can be seen in Fig. 7). A simple optical microscope inspection revealed that the photolithography mask produced using EBL gave a better pattern definition [see Figs. 7 and 5(a)]. The overall production time for the mask printer, including correspondence with a technician, processing time and shipping was at least a week when the cheapest processing and shipment option was selected. The price for the photolithography mask was then about 370 Euro. The estimated cost of making the photolithography mask in our laboratory is about 1200–1500 Euro, based on the price charged for external laboratory users, and it could be done overnight as described. This price can only serve as a guiding figure. The actual price could vary significantly from laboratory to laboratory depending on local equipment depreciation procedures, etc.

TABLE IV. List of how much the write time was improved for each adjustment.

Changed setting	Write time improvement
Increasing aperture size to 120 μm	≈30 times
Selecting high current mode	≈2 times
Meander mode	≈1.5 times
Increase write-field size	≈6 times

VI. CONCLUSION

We present a series of optimized parameter settings, which decrease the writing time for EBL writing with a *Raith e_LiNE* instrument, by more than 40 times compared to most commonly used settings for the instrument. The contributions from the different optimization steps are summarized in Table IV. We have used this method for fabricating chrome photolithography master masks with a write resolution of 200 nm, which we verified by a separate series of line width measurements (not shown). This resolution is about 10 times better than top and bottom what is available with commercial photolithography mask printing, and finer resolution may well be possible. Chrome mask structures up to 15 mm in diameter were written successfully, in less than 8 h and 45 min. Comparing the two fabrication methods revealed more well defined structures for the EBL, as expected, given the higher resolution compared to commercial mask printing. The additional resolution was crucial for the experiment for which the mask was produced.[18]

ACKNOWLEDGMENTS

The authors thank Trond Mohn with Bergens Research Foundation for generous support in setting up the UiB Nanostructures laboratory. This work was also supported by the Norwegian Research Council, Nanomat Project through the programs Nærings-Ph.d., Nanomat Toolplatform and Gaveforstærkning.

[1] S. Kawata, H. Sun, T. Tanaka, and K. Takada, Nature **412**, 697 (2001).
[2] M. Deubel, G. von Freymann, M. Wegener, S. Pereira, K. Busch, and C. Soukoulis, Nature Mater. **3**, 444 (2004).
[3] M. Campbell, D. Sharp, M. Harrison, R. Denning, and A. Turberfield, Nature **404**, 53 (2000).
[4] R. Seliger and W. Fleming, J. Appl. Phys. **45**, 1416 (1974).
[5] R. Piner, J. Zhu, F. Xu, S. Hong, and C. Mirkin, Science **283**, 661 (1999).
[6] R. Menon, A. Patel, D. Gil, and H. Smith, Mater. Today **8**, 26 (2005).
[7] R. F. Pease, Microelectron. Eng. **78–79**, 381 (2005).
[8] J. K. W. Yang, B. Cord, H. Duan, K. K. Berggren, J. Klingfus, S. W. Nam, K. B. Kim, and M. J. Rooks, J. Vac. Sci. Technol. B **27**, 2622 (2009).
[9] M. Kirchner and M. Kahl, Acta Phys. Pol. A **116**, S198 (2009).
[10] E. Abbe, Archiv für Mikroskopische Anatomie **9**, 413 (1873).
[11] A. Broers, A. Hoole, and J. Ryan, Microelectron. Eng. **32**, 131 (1996).
[12] C. Vieu, F. Carcenac, A. Pepin, Y. Chen, M. Mejias, A. Lebib, L. Manin-Ferlazzo, L. Couraud, and H. Launois, Appl. Surf. Sci. **164**, 111 (2000).
[13] T. H. P. Chang, M. G. R. Thomson, E. Kratschmer, H. S. Kim, M. L. Yu, K. Y. Lee, S. A. Rishton, B. W. Hussey, and S. Zolgharnain, J. Vac. Sci. Technol. B **14**, 3774 (1996).
[14] T. Chang, M. Mankos, K. Y. Lee, and L. P. Muray, Microelectron. Eng. **57–58**, 117 (2001).
[15] A. Pepin, V. Studer, D. Decanini, and Y. Chen, Microelectron. Eng. **73–74**, 233 (2004).
[16] B. Bilenberg, S. Jacobsen, M. Schmidt, L. Skjolding, P. Shi, P. Bøggild, J. Tegenfeldt, and A. Kristensen, Microelectron. Eng. **83**, 1609 (2006).
[17] L. E. Ocola and A. Stein, J. Vac. Sci. Technol. B **24**, 3061 (2006).
[18] M. M. Greve, A. M. Vial, and B. Holst, "The beynon gabor zone plate: A new tool for de Broglie matter waves and hard x-rays," (unpublished).
[19] A. Olkhovets and H. G. Craighead, J. Vac. Sci. Technol. B **17**, 1366 (1999).

[20]D. Rio, C. Constancias, M. Saied, B. Icard, and L. Pain, J. Vac. Sci. Technol. B **27**, 2512 (2009).
[21]A. Tilke, M. Vogel, F. Simmel, A. Kriele, R. H. Blick, H. Lorenz, D. A. Wharam, and J. P. Kotthaus, J. Vac. Sci. Technol. B **17**, 1594 (1999).
[22]S. Yasin, D. Hasko, and H. Ahmed, Microelectron. Eng. **61–62**, 745 (2002).
[23]G. Piaszenski, "Application Department, Raith GmbH," personal communication (2012).
[24]H. Jaksch and J. P. Vermeulen, Adv. Mater. Process **116**, 33 (2005).
[25]J. A. Liddle *et al*., J. Vac. Sci. Technol. B **19**, 476 (2001).
[26]J. P. Ballantyne, J. Vac. Sci. Technol. **12**, 1257 (1975).